7-2013

Production of O(1D) following electron impact on CO2

Wladyslaw Kedzierski
University of Windsor

J. D. Hein

C. J. Tiessen

D. Lukic

J. A. Trocchi

See next page for additional authors

Recommended Citation

Kedzierski, Wladyslaw; Hein, J. D.; Tiessen, C. J.; Lukic, D.; Trocchi, J. A.; Mlinaric, T. Z.; and Mcconkey, J. W.. (2013). Production of O(1D) following electron impact on CO2. *Canadian Journal of Physics*, 91 (12), 1044-1048.
https://scholar.uwindsor.ca/physicspub/186

Production of $O(^1D)$ Following Electron Impact on CO_2

W Kedzierski, J D Hein*, C J Tiessen, D Lukic, J A Trocchi, T Z Mlinaric and J W McConkey

Physics Department, University of Windsor, ON N9B 3P4, Canada.

Abstract:

We have studied the excitation of metastable $O(^1D)$ following dissociative excitation of CO_2 in the electron impact energy range from threshold to 400 eV. A solid Ne matrix at ~20K forms the heart of the detector. This is sensitive to the metastable species through the formation of excited excimers (NeO*), The resultant excimer radiation is readily detected, providing a means of measuring the production of the metastables. Using a pulsed electron beam and time-of-flight techniques, we have measured the $O(^1D)$ kinetic energy spectrum and its relative production cross sections as a function of electron impact energy. Threshold energy data are used to gain information about the excitation channels involved. In addition, an emission excitation function for the red photons, emitted in coincidence with the exciting electron pulse, has been measured in the 0-400 eV energy range.

PACS #s 34.80 Dp and Ht, 33.20 kf, 37.20 +j, 34.35 +a

*Current address: Jet Propulsion Laboratory, California Institute of Technology, Pasadena, CA 91109, USA.

1. Introduction:

Metastable O(^1D) atoms are an important constituent of the terrestrial atmosphere where the well known 'nebular' red lines at 630 and 636.4 nm in the airglow and auroral spectra result from O(^{1}D – ^{3}P) decay. Both the intensity and polarization of the red lines have proved to be significant [1,2]. A major source of O(^1D) atoms in the atmosphere is photo-dissociation of O_2 or O_3 by solar ultraviolet photons. O(^1D) plays a vital role in earth's atmosphere through quenching processes, which lead to heating, and chemical reactions which modify its chemical composition, particularly in the stratosphere [3-5]. Beyond earth's environment, O(^1D) is an active participant in cometary processes [6], and the red lines are prominent features of many nebulae [7]. Metastable oxygen, including O(^1D), is also important in any plasma or discharge situation involving oxygen containing gases [8,9].

Because of its long (116 sec) lifetime [10], single particle detection of O(^1D) in the laboratory is very difficult although it is readily possible to excite the red lines in a discharge by using a buffer gas to reduce wall deactivation [11]. Techniques which have been successful are usually laser or synchrotron based, where ionization of O(^1D) is used as a precursor to mass spectroscopic detection of the resultant O^+, [12,13]. Recently, Kedzierski *et al.* [14,15], have demonstrated that it is possible to carry out single particle detection of both low-lying metastable oxygen species, O(^1D) and O(^1S), using rare gas matrix detectors. Here the metastable atom strikes a solid rare gas (Rg) matrix surface (e.g., Ne, Ar, Kr, or Xe) and forms an RgO* excimer which promptly radiates.

The technique of using excimer formation in a solid rare gas matrix to shorten the lifetimes of metastable atoms dates back to earlier work where small quantities of oxygen containing molecules were frozen out in solid deposits of rare gases and then bombarded with electrons or energetic photons [16-25]. Ne was identified in this earlier work [18,20,24,25] as being different from the other rare gas matrices in that the spin-forbidden, magnetic dipole (^1D - ^3P) emission was observed in addition to the electric quadrupole (^1S – ^1D) line when VUV photon irradiation of matrices containing traces of O_2, N_2O or CO_2 was carried out. More recently, Belov *et al.* [26], used 2 keV electron bombardment of Ne crystals containing a trace of

O_2 and confirmed that the (^1D - ^3P) emission was observed from the matrix in that situation also.

Photon (as distinct from electron) dissociation of CO_2, with production of O(^1D), dates back to the early pioneering work of Slanger and Black [27,28]. Stolow and Lee [12] studied the break-up of CO_2 at 157.6 nm using a crossed beam technique and a mass spectrometer detector, and confirmed earlier work, using LIF [29] and chemical scavenging [30] techniques. They found that the dominant reaction pathway at this wavelength is

$$CO_2(^1\Sigma_g^+) \rightarrow CO(^1\Sigma^+) + O(^1D) \qquad (1)$$

with a quantum yield of 0.94 and an angular anisotropy parameter, β, of zero. More recently, Lu *et al.* [13] obtained similar results using photo-fragment translational spectroscopy where the ionization stage was accomplished using VUV synchrotron radiation. The quenching of O(^1D) by various molecules has been studied [31-33] and Perri *et al.* [34] have studied the fine detail of this process when the quenching partner is CO_2.

The present report extends our earlier work [15] on the use of the Ne matrix for O(^{1}D) detection. The electron-CO_2 production of O(^{1}D) is investigated in detail. Use of electrons rather than photons, as the initiators of the dissociation process, opens the door to additional non-dipole excitation channels.

2. Experimental Techniques.

The apparatus and technical details are very similar to those used in earlier work [14,15] so only a brief summary will be presented here. A two-chamber differentially pumped vacuum system houses the experiment (see [14] for a diagram of the apparatus). Turbo-molecular pumps provide a base pressure of less than 10^{-6} torr in the main chamber which contains the differentially-pumped, magnetically confined, pulsed electron beam and target gas inlet system. Dissociation fragments from the electron-target interaction progress pass into the second chamber which contains a cold finger held at a controlled temperature by an Advanced Research Systems, Inc. DE-202 cryogenic unit. This unit also serves as a cryopump for the second chamber. Neon is leaked into this chamber and

directed towards the cold finger surface where a solid neon matrix slowly accumulates when the temperature is reduced to below 30K. Oxygen metastables incident on this cold surface thermalise, form NeO* excimers and radiate. Some loss of O(^1D) metastables may occur en route from the interaction region to the detector due to background CO_2 which is an effective quencher of O(^{1}D) [32] but any background Ne should have negligible effect [32]. A fraction of the resultant photons from the cold finger are detected by an R943-02 Hamamatsu photomultiplier, cooled to -30˚C, and the pulses are routed to a Stanford Research Systems SR430 multichannel scaler (MCS). In the case of RgO(^1D) the excimer emission coincides in wavelength with the atomic O-line emission i.e. close to 630 nm. A suitable red glass filter which blocks any radiation below about 600 nm allows transmission of the red excimer emission but blocks detection of the RgO(^1S) green emission [14] from the detector surface. The electron beam is pulsed (pulse length ~20 μs, repetition rate 500 Hz) and has a typical equivalent DC current of 100 μA. The excitation to (and subsequent de-excitation from) optically allowed states produces "prompt" photons in coincidence with the electron beam pulse. These start the MCS sweep and establish the zero of the time scale. A short time later the metastables arrive at the detector and give rise to the metastable time-of-flight (TOF) spectrum.

A sample of the TOF data obtained is shown in Figure 1where the incident electron energy is 100 eV. This picture is the sum of many such spectra taken at this electron energy representing many days of data acquisition. Due to the poor detector sensitivity the metastable signal is quite weak so that the prompt photon peak dominates the spectrum. Using the SR430, specific time windows can be selected and the accumulated counts can be monitored as the electron energy is ramped. This allows the probability of production of the species under investigation to be measured as a function of impact energy thus producing a so-called "excitation function". Because of low signal levels and resultant rather poor statistics these measurements were augmented by individual measurements taken at constant electron energy in which the integrated metastable signal was obtained from the TOF graph. A composite of these two methods is shown in the next section. By selecting a time window at shorter times the excitation function of the prompt photon signal could also be obtained. The electron beam current was

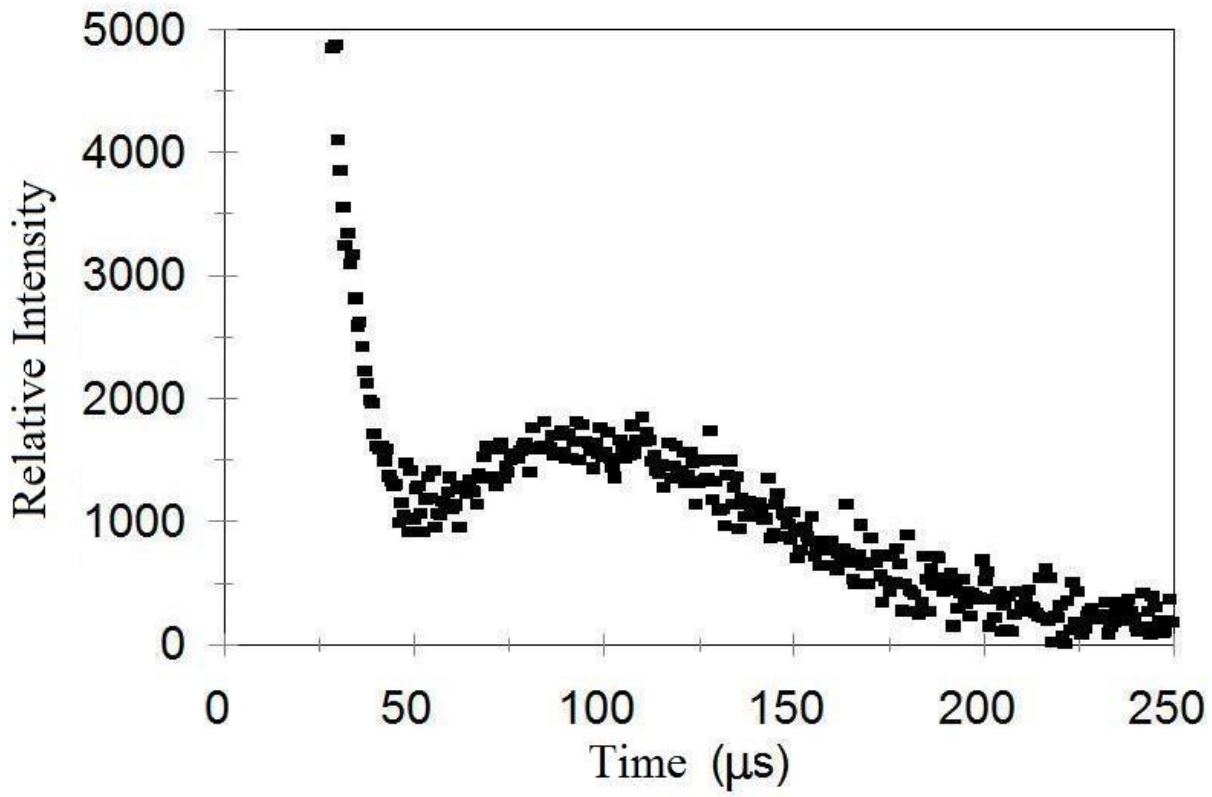

Fig 1. TOF signal following 100 eV electron impact on CO_2. Note the dominant (off-scale) prompt photon peak at short times .

carefully monitored as the energy was varied so that normalization of the data to constant beam current could occur.

3. Results and Discussion.

3.1. TOF and Kinetic Energy Data.

As seen in the TOF spectrum in Figure 1, a non-negligible tail from the prompt photon signal encroaches on the metastable signal. To accurately measure metastable signal from TOF data, this underlying prompt photon signal must be accounted for. There are two ways we have developed to accomplish this.

We first take an additional data set at the same electron energy and other experimental conditions but with a clear glass slide blocking the line-of-sight between the interaction region and the cold finger. This allows the prompt photons to pass but blocks the metastables. From this, a TOF curve is produced which exhibits only the prompt photon signal. Alternatively we have fitted an exponential to the prompt photon decay signal to enable its contribution at longer times to be obtained. Using either of these techniques we can subtract the photon signal from spectra such as in Figure 1and get a TOF curve for the metastables on their own. Such a curve is shown in Figure 2. Both techniques yielded very similar results.

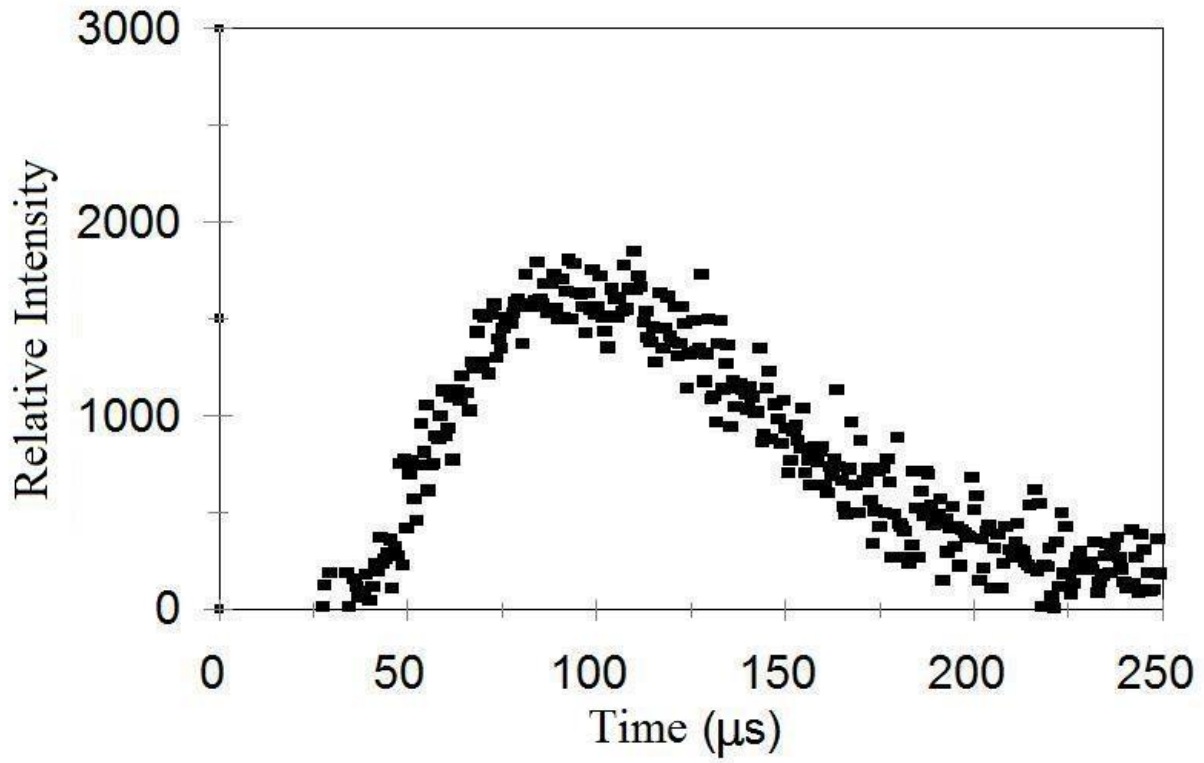

Fig. 2. O(^1D) TOF data obtained using 100 eV electron impact on a CO_2 target where the prompt photon signal has been removed by techniques as described in the text. The e-beam pulse width was 25μs and the target head gas pressure was 11 Torr.

There is no obvious structure present in the TOF spectrum, Fig. 2. We contrast this to what was observed by LeClair et al [35], for O(^1S) production from this target. There, six features were evident following 100 eV electron impact indicating at least this number of channels were contributing to the observed signal. Here, the apparent lack of structure is probably a product of the poorer statistics and the much broader electron pulse which had to be used in the present work. Thus any structure present in the data could be "washed out".

Knowing the mass of the metastable particle and the distance travelled to the detector, the data shown in Fig 2 can be converted to a graph of signal versus kinetic energy, T, of the O(^1D) fragment using the procedure outlined by Smyth et al [36]. In practice, because of the rather poor statistical significance of the data (Fig 2) we need to carry out significant smoothing of the converted data particularly at the lowest energies (longest TOFs). As an alternative procedure, we first fitted a curve to the data in Fig 2 and then carried out the transformation using this fitted curve. Both methods gave very similar results. The result is shown in Fig 3. If the target dissociates into only two fragments then, using conservation of momentum, the total released kinetic energy, E, is given by $E = T[M/m]$ where M denotes the total mass of the target and m the mass of the undetected fragment. For the dissociation defined by Equation 1, the multiplying factor is [44/ 28 = 1.57]. Thus while the maximum in the O(^1D) kinetic energy spectrum occurs close to 0.4 eV, the maximum in the total kinetic energy release curve would be more than 0.6 eV with a tail extending well beyond 3 eV. We note that these numbers are rather similar to those observed by LeClair and McConkey [37] in their study of O(^1S) production from CO_2. Further, we note that Stolow and Lee [12], in their photodissociation study at 157 nm leading to O(^1D) production, found kinetic energy releases of up to 0.5 eV with significant rotational and vibrational excitation of the molecular CO partner fragment as well.

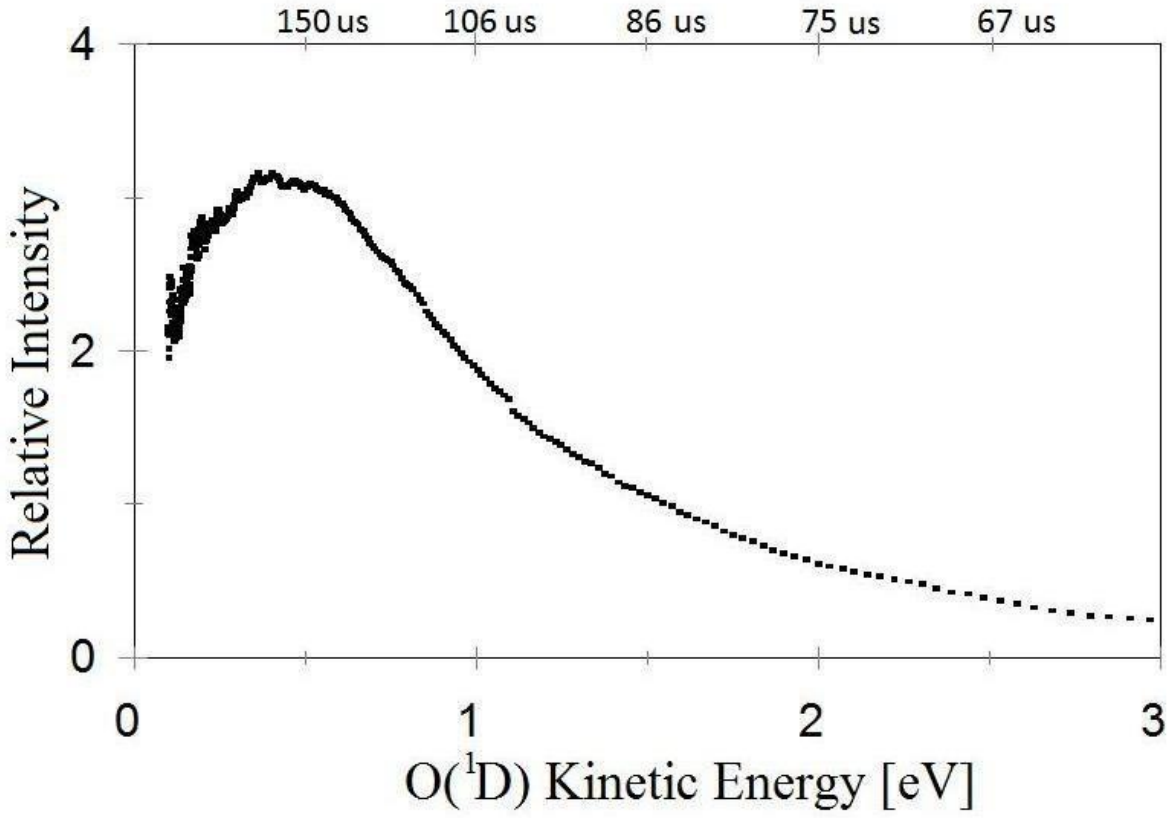

Fig. 3. O-fragment kinetic energy transform of the data shown in Fig 2. Some smoothing of the raw data has been applied. Note that the plot has been truncated at the lowest energies because of the noise in the TOF data at the longest flight times. For convenience some flight times are included on the top of the figure.

3.2. Excitation Functions.

By selecting TOF windows and varying the incident electron energy, as discussed in the experimental section, we obtain the data sets shown in Figs 4 and 5 for prompt photons and metastable O(^1D) atoms respectively.

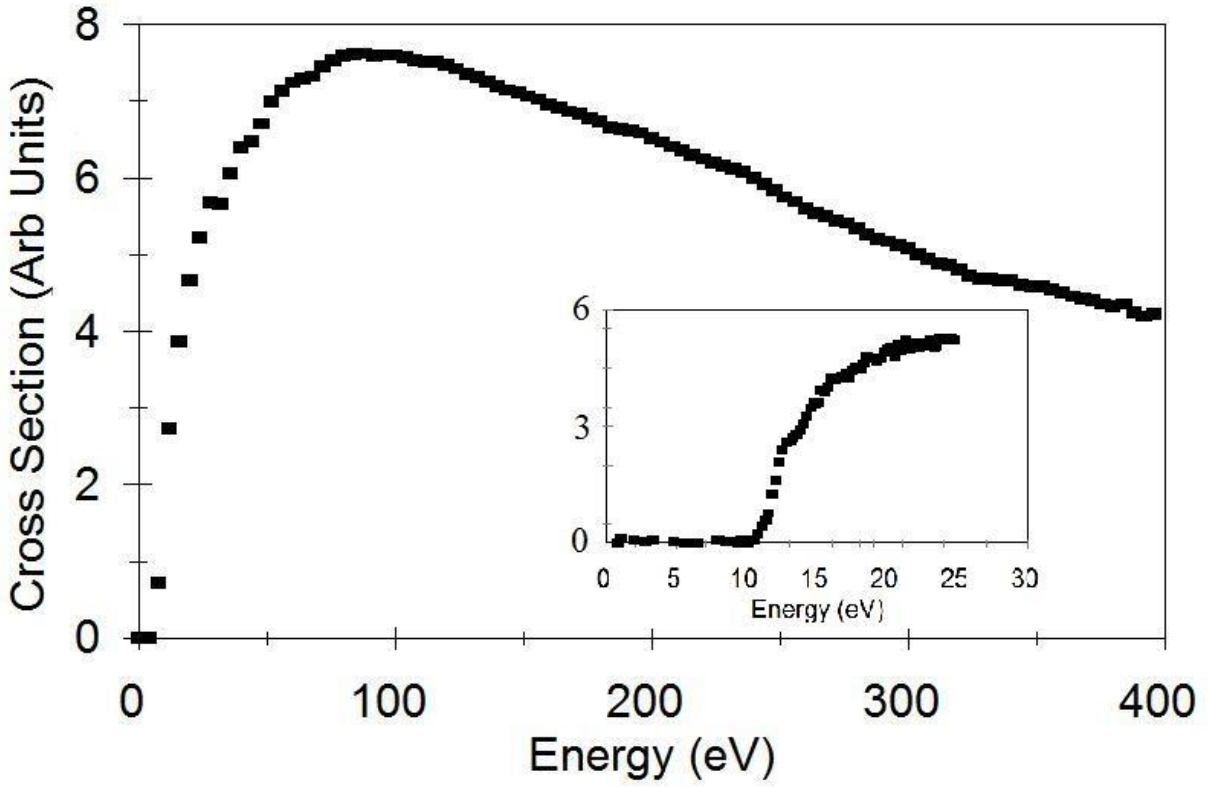

Figure 4. Excitation probability for prompt red photon production following electron impact on CO_2. The insert shows the near-threshold data. See text for further details.

Consider first the prompt photon data. We note first of all that only emissions falling within the wavelength window defined by the filter cut off and the high-wavelength fall off in sensitivity of the photomultiplier (approximately between 600 and 1000 nm) need be considered. Excitation of CO_2 by electron impact has been surveyed by McConkey et al [38] who found that the only significant atomic spectral features in this spectral range were due to the 3p $^5P \rightarrow$ 3s ^5S and 3p $^3P \rightarrow$ 3s ^3S transitions of atomic oxygen at 777.4 and 844.6 nm respectively. The emission cross sections of these lines at 100 eV had been measured by Zipf [39]. The minimum energies required to excite these lines are 16.17 and 16. 41 eV respectively. Here zero kinetic energy of the fragments has been assumed and no excitation of the unobserved fragment(s) is assumed to occur. The dissociation energy of CO_2, D(CO + O), is a contribution of 5.45 eV to these figures. If we assume a similar amount of kinetic energy release to what is observed using the metastable data (Fig 3) then we might expect the threshold for the atomic prompt

photon signal to occur near 16.5 eV. However there is also the possibility of detection of ro-vibrational radiation from molecules which were excited in the electron collisions. This radiation could be observed at energies below the threshold for atomic excitation. So in order to fix the electron energy scales on Figs 4 and 5, we used the threshold for excitation for O(^1S) production under identical experimental conditions. This had been measured by LeClair *et al* [37] to be 11.0 ± 0.5 eV. A more accurate energy calibration is unwarranted given the assumptions used above and the ~1 eV spread in the electron beam energy resolution. Using this calibration the threshold for prompt photon production was measured to occur at 11.5 eV confirming that indeed some molecular radiation was being observed.

The excitation function, Fig 4, reveals a sharp rise from threshold, suggestive of a spin-flip in the excitation of the parent molecular state, followed by a broad maximum around 100 eV suggesting that, in addition, there are strong optically allowed components in the excitation. A discontinuity occurs about 16 eV above the first threshold, i.e. at 27.5 eV. Total fragmentation of the molecule with excitation of one of the O atoms requires at least 27.4 eV, so a likely candidate process here could be

$$e + CO_2 \rightarrow C(^3P) + O(^3P) + O^*(^3P \text{ or } ^5P) \qquad (2)$$

Because of the low O(^1D) signal the statistical significance of the data, Fig 5, taken by ramping the electron energy and monitoring the signal within the 75-175 μs TOF window that included the metastable signal, was rather low. The data were however sufficiently good to demonstrate that the onset energy for O(^1D) production occurred below the threshold for prompt photon production at 11.5 eV. The additional data shown in Fig 5 were taken at individual energies by obtaining TOF curves and integrating the signals in the metastable peaks. Individual points were normalized to take account of any variations in beam current, source pressure or data acquisition time. TOF data at 100 eV were taken at numerous times during the entire data taking period to check for any variation of the efficiency of the detection system with time or Ne layer thickness. Unfortunately due to a lack of knowledge of the absolute sensitivity of the detector to O(^1D), it was not possible to absolutely calibrate the relative excitation function, Fig 5.

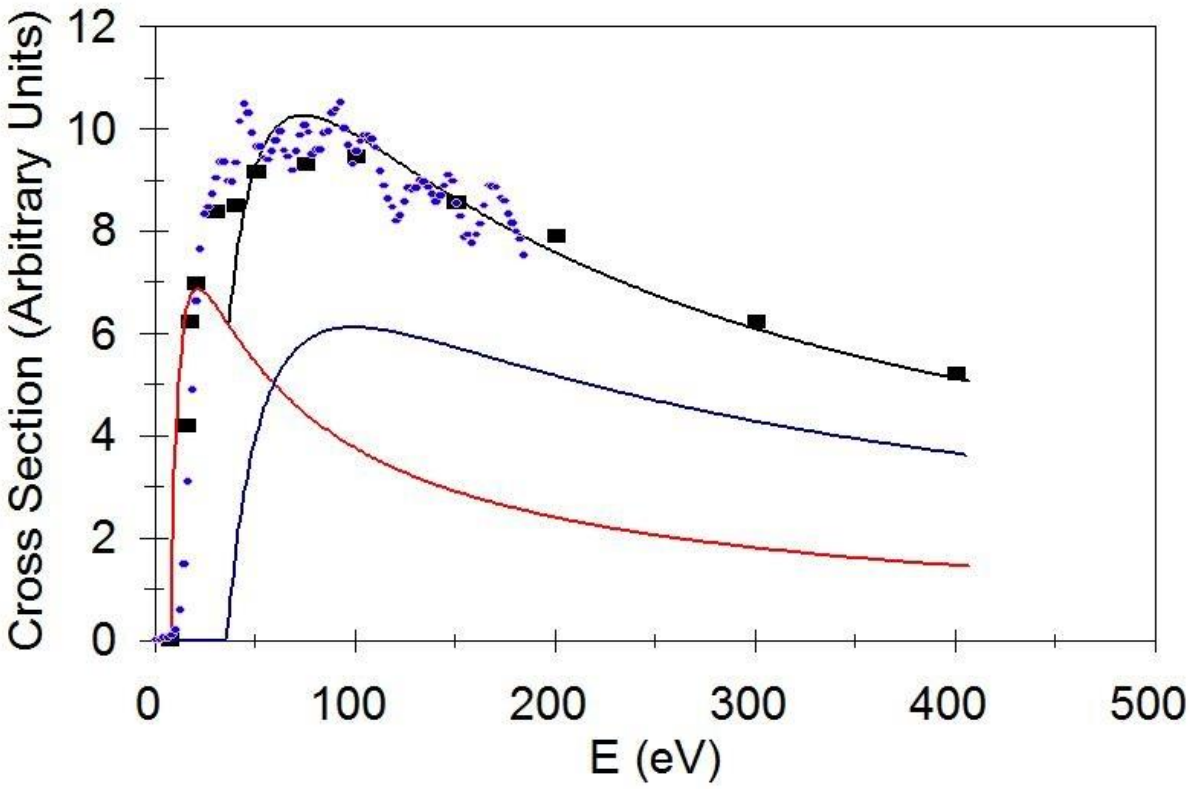

Figure 5. Excitation probability for O(^1D) production from CO_2 as a function of impact electron energy. The dots represent data where the impact electron energy was ramped. The solid squares indicate data taken at particular impact energies. The solid curves indicate a possible breakdown of the plot into its individual components. See text for further details.

Although the statistical quality of the data in Fig 5 is not good, a number of points are still evident. As discussed above, the excitation threshold occurs at 8±1 eV. This is consistent with the calculated threshold for O(^{1}D) production of 7.66 eV if zero kinetic energy is released at threshold. We know from photon impact work [e.g.,12] that the dipole channel is open by 7.86 eV and so the first onset in the data, Fig 5, is consistent with the opening of this channel.

Fig 5 also shows an attempt to fit the data to a combination of theoretical curves representative of the type of processes which may be occurring. The Bethe-Born approximation predicts that the high-energy cross section varies as ln$E$/E, 1/E, and 1/E^3 for the optically allowed, optically forbidden but spin allowed or spin-forbidden excitations, respectively, where E is the kinetic energy of the incident

electron. To separate the total excitation function into its individual channels and determine each threshold energy, we tried to use the procedure discussed by Brotton and McConkey [40] where the following formula is fitted to the data in Fig 5:

$$\sigma = \sum_{j=1}^{m} A_{ij} \frac{\ln X_{ij}}{X_{ij}} + \frac{X_{ij} - 1}{X_{ij}} \left(\frac{B_{ij}}{X_{ij}} + \frac{C_{ij}}{X_{ij}^3} \right) \qquad (3)$$

The subscripts *i* and *j* denote the initial CO_2 ground state and a particular intermediate excited molecular state CO_2^*, respectively, *m* is the number of intermediate states or individual channels, and $X_{ij} = E/E_{ij}$ with E_{ij} denoting the initial excitation energy. The factor of $(X\text{-}1)/X$ ensures that the cross section σ decreases linearly towards zero [$\sigma \propto X(A+B+C)$] as the threshold energy is approached ($X \rightarrow 1$). The adjustable parameters in the fit are the A_{ij}, B_{ij}, C_{ij}, and E_{ij}. Equation (3) is exact only in the limit of high energies *E*.

Unfortunately the statistical quality of the data was insufficient to justify the use of such a multi-parameter fit as defined by Equation 3 and so we proceeded as follows. We know that a dipole allowed process is active right from the initial threshold and we also know, (see below), from the high energy behavior of the data, that dipole allowed processes are dominant there also. Thus the fit to the data given in Fig 5 consists of two dipole allowed channels. The onset of the higher energy channel is found to occur at ~34 eV.

To show that the excitation function is dominated by a dipole contribution at high energy we plot the data of Fig 5 on a so-called Bethe plot of σE vs ln *E*, Fig 6. A positive slope towards high energies , such as is seen in Fig 6, is indicative of dipole allowed excitation in the parent molecule [41].

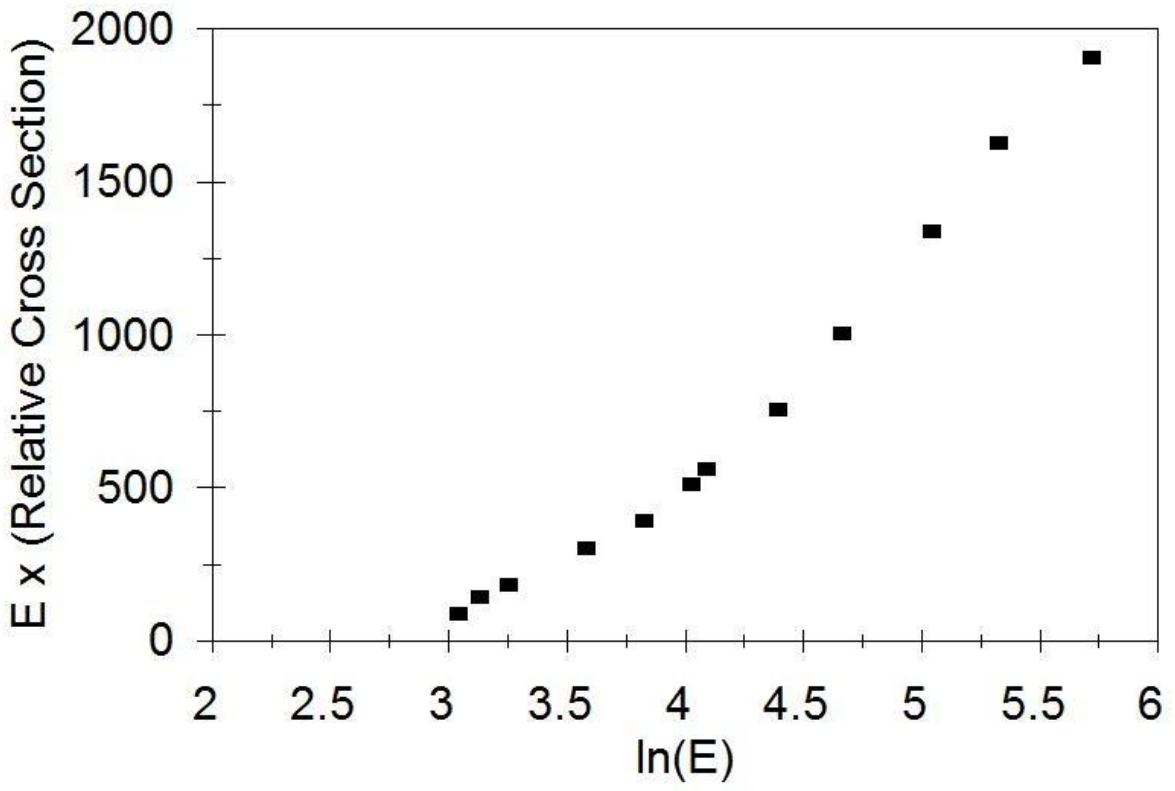

Figure 6. Bethe plot of the data in Fig 5. See text for further details.

A possible candidate for the higher energy process is one where total fragmentation of the molecule occurs, namely

$$e + CO_2 \rightarrow C(^3P) + O^+(^4S) + O(^1D) \qquad (4)$$

The calculated threshold for this with no release of kinetic energy is 32.13 eV

Conclusions.

Production of $O(^1D)$ following electron impact dissociation of CO_2 has been studied in the electron energy range from threshold to 400 eV using a novel Ne-matrix detector at a temperature of ~20K. $O(^1D)$ fragment kinetic energies as a result of the dissociation have been measured to maximize at ~0.4 eV but to range

up to approximately 3 eV. From the shape of the excitation function it appears that at least two dipole excitation processes in the parent molecule are contributing.

A relative emission cross section for the near infrared radiation from the CO_2 molecule, including the 3p $^5P \rightarrow$ 3s ^5S and 3p $^3P \rightarrow$ 3s ^3S transitions of atomic oxygen at 777.4 and 844.6 nm respectively and also some molecular radiation, has been obtained for the first time.

Acknowledgements.
Financial support for this work from the Natural Sciences and Engineering Research Council of Canada is gratefully acknowledged. CJT, DL and JAT and TZM acknowledge support from the University of Windsor "Outstanding Scholars" program. Expert technical help was obtained from the University of Windsor, Physics Department mechanical and electronic shops.

4. References:

[1] J Lilensten et al, Geophys Res Lett, **35**, 8804, (2008).
[2] V Bommier, S Sahal-Brechot, J Dubau and M Cornille, Ann Geophys, **29**, 71, (2011).
[3] M.H. Rees, "Physics and chemistry of the upper atmosphere" Cambridge University Press (1989).
[4] V. Kharchenko, A. Dalgarno, J.L. Fox, J. Geophys. Res. **110**, A12305, (2005).
[5] S Vranckx, J Peeters and S Carl, Phys Chem Chem Phys, **12**, 9213, (2010).
[6] A. Bhardwaj and S.A. Haider, Adv. Space Res. **29**, 745, (2002).
[7] G.S. Khromov, Soviet Astronomy **9**, 431, (1965).
[8] G Borcia, R Cazan and G Popa, IEEE Trans Plasma Sci, **39**, 2102, (2011).
[9] M Nikolic, S Popovic, J Upadhyay, L Vuskovic, R Leiweke and B Ganguly, Plasma Sources Sci Tech, **21**, 015004, (2012).
[10] B.D. Sharpee and T.G. Slanger, J. Phys. Chem. A **110** , 6707, (2006).
[11] J.W. McConkey, R.E.W. Pettifer, K.A. Moran, Planet. Space Sci. **18** , 771, (1970).
[12] A. Stolow and Y.T. Lee, J. Chem. Phys. **98** , 2066, (1993).
[13] I.-C. Lu, J.J. Lin, S.-H. Lee, Y.T. Lee, X. Yang, Chem. Phys. Letts. **382**, 665, (2003).
[14] W. Kedzierski, E. Blejdea, A. DiCarlo, J.W. McConkey, J. Phys. B **43**, 085204, (2010).

[15] W. Kedzierski, E. Blejdea, A. DiCarlo, J.W. McConkey, Chem Phys Lett, **498**, 38, (2010)
[16] L. Schoen and H.P. Broida, J. Chem. Phys. **32** (1960) 1184.
[17] R. Taylor, W. Scott, P.R. Findley, Z. Wu, W.C. Walker, K.M. Monaghan, J. Chem. Phys. **74** (1981) 3718.
[18] W.C. Walker, R.V. Taylor, K.M. Monahan, Chem. Phys. Letts. **84** (1981) 288.
[19] W.G. Lawrence and V.A. Apkarian, J. Chem. Phys. **97** (1992) 2229.
[20] D. Maillard, J. Fournier, H.H. Mohammed, C. Girardet, J. Chem. Phys. **78** (1983) 5480.
[21] C. Girardet, D. Maillard, J. Fournier, J. Chem. Phys. **84** (1986) 4429.
[22] J. Goodman, J.C. Tully, V.E. Bondybey, L.E. Brus, J. Chem. Phys. **66** (1977) 4802.
[23] A.G. Belov and E.M. Yurtaeva, Low Temp. Phys. **27** (2001) 938.
[24] D. Maillard, J.P. Perchard, J. Fournier, H.H. Mohammed, C. Girardet, Chem. Phys. Letts. **86** (1982) 420.
[25] J. Fournier, H.H. Mohammed, J. Deson, D. Maillard, Chem. Phys. **70** (1982) 39.
[26] A.G. Belov, I.Y. Fugol, E.M. Yurtaeva, O.V. Bazhan, J. Lumin. **91** (2000) 107.
[27] T. Slanger and G. Black, J. Chem. Phys. **54** (1971) 1889.
[28] T. Slanger and G. Black, J. Chem. Phys. **68** (1978) 1844.
[29] R. Miller, S.H. Kable, P.L. Houston, I. Burak, J. Chem. Phys. **96** (1992) 332.
[30] Y.F. Zhu and R.G. Gordon, J. Chem. Phys. **92** (1990) 2897.
[31] E.J. Dunlea and A.R. Ravishankara, Phys. Chem. Chem. Phys. **6** (2004) 2152.
[32] J A Davidson et al, J Chem Phys, 64, (1976), 57.
[33] G.E.Streit et al, J Chem Phys, 65, (1976), 4761.
[34] M.J. Perri, A.L. Van Wyngarden, J.J. Lin, Y.T. Lee, K.A. Boering, J. Phys. Chem. A **108** (2004) 7995.
[35] L.R. LeClair, M.D. Brown, J.W. McConkey, Chem. Phys. **189** (1994) 769.
[36] K. Smyth, J.A. Schiavone, R.S. Freund, J. Chem. Phys. **59** (1973) 5225.
[37] L.R. LeClair, and J.W. McConkey, J. Phys B, **27**, (1994), 4039.
[38] J W McConkey et al, Phys Rep, **466**, (2008), 1.
[39] E.C.Zipf in *Electron-Molecule Interactions and their Applications,* Ed L.G.Christophorou, Academic Press, New York, **1**, (1984), 335.
[40] S.J.Brotton and J W McConkey, J Phys B, **44,** (2011), 215202.
[41] M Inokuti, Rev Mod Phys, 43, 297, (1971).